

Tailoring Magnetic Properties of CoFeB Films via Tungsten Buffer and Capping Layers

L. Saravanan^{1*}, Nanhe Kumar Gupta², Carlos Garcia¹, and Sujeet Chaudhary²

¹*Departamento de Física, Universidad Técnica Federico Santa María, Valparaíso 2390123, Chile*

²*Thin Film Laboratory, Department of Physics, Indian Institute of Technology Delhi, New Delhi 110016, India*

[*saravanan.lakshmanan@usm.cl](mailto:saravanan.lakshmanan@usm.cl)

Abstract

Controlling the interface between W and CoFeB-based buffer or capping layers at an appropriate temperature is essential for modifying the strength of magnetic anisotropy. In this work, we systematically explore the impact of W buffer and capping layers on the structural, topological, and magnetic anisotropy properties of W (5 nm)/CoFeB(10 nm) and CoFeB(10 nm)/W(3 nm) bilayers sputtered at room temperature (RT) and annealed at an optimal annealing temperature (T_A) of 400°C. Our findings demonstrate that the bilayer films' uniaxial magnetic anisotropy (UMA) with out-of-plane coercivity (H_{cL}) is highly influenced by the W buffer, capping layers, and T_A . Specifically, the H_{cL} of the CoFeB layer with the buffer and capping layers annealed at 400°C samples exceed several times the coercivity of those unannealed. CoFeB buffered with W and annealed at 400°C shows larger H_{cL} , two-fold UMA, and higher in-plane UMA energy density (K_{eff}) than the CoFeB/W bilayers, which can be attributed to the W buffer layer inducing the crystallization of CoFeB during annealing. The W buffer, capping layers, and the T_A for W and CoFeB-based bilayer samples significantly alter the surface morphology, grain sizes, and surface roughness. The XRD analysis reveals nano-crystallites embedded in the larger grains of the 400°C annealed samples. Hence, this work offers a promising approach to achieving high thermal stability of UMA in W and CoFeB-based spintronic applications.

Keywords: Sputtering, CoFeB films, Uniaxial magnetic anisotropy, Out-of-plane coercivity, Spintronics

1. INTRODUCTION

There is a broad interest in studying ultrathin films and nanostructures with perpendicular magnetic anisotropy (PMA) and large H_{cL} for their application in novel spintronic devices. Recent studies have revealed that ultrathin films composed of heavy metal (HM)/ferromagnet (FM) layers can significantly elucidate spin-orbit effects such as Spin-Orbit Torque (SOT) [1] and Dzyaloshinskii-Moriya Interaction (DMI) [2]. The DMI in ultrathin films with specific magnetic anisotropy is critical to enhancing topologically protected spin structures such as magnetic skyrmions [3,4]. The SOT mechanism enables switching the magnetization in a ferromagnetic film by applying a current through an adjacent heavy metal layer or topological insulators [5,6].

The specific properties and interfaces of thin films are heavily influenced by their preparation methods and growth conditions. The properties include lattice mismatches between adjacent layers, crystallographic relationships, surface roughness, surface morphology, interface characteristics, and electronic effects [7,8]. For practical applications, magnetic films must possess adjustable magnetic coercivity, domain structure, and magnetization distribution [9]. This adjustability is achieved through engineering magnetic, buffer, and capping layers, involving thermal treatments, film thickness, and magnetic film composition modifications. Magnetic coercivity values depend on the films' magnetic anisotropy energy, crystal structure, and surface morphology [10–12]. These findings have prompted a systematic investigation into the impact of heavy metal buffers and capping layers with a large Spin Hall Angle (θ_{SHA}) on the magnetic anisotropy of CoFeB films deposited on the suitable substrates. Recent studies have contributed to optimizing the Magnetic Tunnel Junction (MTJ) structures by integrating specific heavy metals such as Ta, Pt, Hf, Mo, Ru, and W as buffer and/or capping layers [13–18]. Specifically, research has shown that a CoFeB/MgO framework with W buffer and capping layers exhibits superior annealing stability compared to a CoFeB/MgO framework with Ta buffer and capping layers [17]. This suggests that incorporating specific heavy metals can enhance the performance and reliability of MTJ structures and offer potential improvements in various applications such as magnetic memory devices and other spintronic technologies.

PMA and/or H_{cL} properties at lower thicknesses of the magnetic layer are crucial for ultrathin film data storage applications [19–21]. Additionally, modern perpendicular MTJs (p-

MTJs) must withstand industrial standard processing temperatures of 400°C necessitating satisfactory thermal stability of the stacks [22,23]. B. Sun *et al.* [24] first reported a significant enhancement in the H_{cL} of the CoFeB layer in Si//CoFeB/Ag structures with a thickness of 172 nm, which is attributed to magnetocrystalline anisotropy. Additionally, the effect on H_{cL} of thickness, buffer and capping layers of Ta or W in CoFeB films have been previously investigated [25–27]. A significantly high value of H_{cL} of 1250 Oe was reported for W/CoFeB/W at 400°C trilayer films [27]. However, the development of CoFeB films with W buffer and capping layers alone and a comprehensive study of their structural, surface morphological and magnetic properties have not yet been reported. From both fundamental and technological perspectives, examining interface-induced H_{cL} in designing multilayer structures with relatively thick CoFeB films is relevant to understanding the role of W capping and buffer layers in tailoring magnetic properties and optimizing hard-axis coercivity for advanced spintronic devices. Thicker CoFeB films are a model for studying fundamental magnetic properties such as spin waves, domain walls, and magnetization dynamics. Specifically, the study of 10 nm thickness CoFeB films is significant because i) it provides a high surface-to-volume ratio, ii) it leads to low power consumption in spintronic devices, iii) it enhances fast magnetization dynamics for high-speed applications, and iv) it ensures compatibility with existing semiconductor manufacturing processes.

This study reports the structural, magnetic anisotropy, and surface morphological properties of W(5 nm)/CoFeB(10 nm) and CoFeB(10 nm)/W(3 nm) bilayers annealed at an optimal temperature of 400°C. The findings highlight the critical role of tungsten buffer and capping layers in tuning uniaxial magnetic anisotropy and enhancing hard axis coercivity.

2. EXPERIMENTAL DETAILS

Bilayer films were fabricated on thermally oxidized (500 nm SiO₂) Si substrates [sizes = 1 × 1 square inch] using the pulsed DC magnetron sputtering technique at RT. After preparation, samples were immediately characterized to minimize the formation of surface impurities. Two types of heterostructures were deposited:

- I. SiO₂//W (5 nm)/CoFeB(10 nm)
- II. SiO₂//CoFeB(10 nm)/W(3 nm)

The base pressure in the sputtering chamber was maintained below 1.0×10^{-6} Torr. The sputtering targets of $\text{Co}_{20}\text{Fe}_{60}\text{B}_{20}$ and W with high purity (99.99%) were used to grow the respective bilayers. The ferromagnetic CoFeB layer was deposited using a DC power of 40 W and an Ar pressure of 3.2 mTorr. The heavy metal W layer was sputtered at a DC power of 10 W and an Ar pressure of 3.2 mTorr. The sputtering rates for CoFeB and W were 0.83 \AA/s and 0.26 \AA/s , respectively. After deposition, the bilayers underwent *ex-situ* annealing at the optimal temperature of 400°C for 60 minutes in a vacuum environment below 4.0×10^{-5} Torr without applying any magnetic field.

The crystal structure of the bilayer films was analyzed using Grazing Incidence X-ray Diffraction (GI-XRD) with a *PANalytical X'pert PRO* diffractometer and employing Cu K_α radiation ($\lambda = 1.5406 \text{ \AA}$). The thickness of the individual layers within the structure was determined through X-ray Reflectivity (XRR) measurements using the same diffractometer with the *X'Pert Reflectivity, v1.2a* software. The elemental composition of the CoFeB films (Co: Fe: B = 20: 60: 20) was confirmed by Energy Dispersive Spectroscopy (EDS) coupled with Scanning Electron Microscopy (SEM) [*Hitachi High Technol*]. The magnetic anisotropy measurements were conducted at RT using a home-built longitudinal Magneto-Optical Kerr Effect (L-MOKE) setup. This instrument utilized a linearly polarized intensity stabilized He-Ne laser source ($\lambda = 632 \text{ nm}$) with a laser spot diameter of less than $500 \text{ }\mu\text{m}$ [28]. The angular dependence of the squareness ratio (M_r/M_s) was determined by recording MOKE M-H loops at different in-plane azimuthal orientations of the applied magnetic field. In-plane and out-of-plane DC magnetization hysteresis loops were also recorded at RT using the Vibrating Sample Magnetometer (VSM) [*Microsense EZ11 VSM*]. The surface morphology of the samples was examined using Atomic Force Microscopy (AFM) [*Asylum Research MFP3D-SA*] in tapping mode.

3. RESULTS AND DISCUSSION

3.1 Thin film thickness measurement

Fig. 1 (a)-(b) schematically illustrates the two types of fabricated heterostructures comprising layers of W and CoFeB-based sputtered on SiO_2 (500 nm) substrates. The CoFeB layer thicknesses are estimated from XRR fitting and aligned well with the nominal film thickness of 10 nm. To accurately determine the thickness of each layer, XRR measurements

were conducted on all the as-dep. or RT bilayer films as shown in Fig. 1(c). The fitted XRR spectra closely match the observed experimental data.

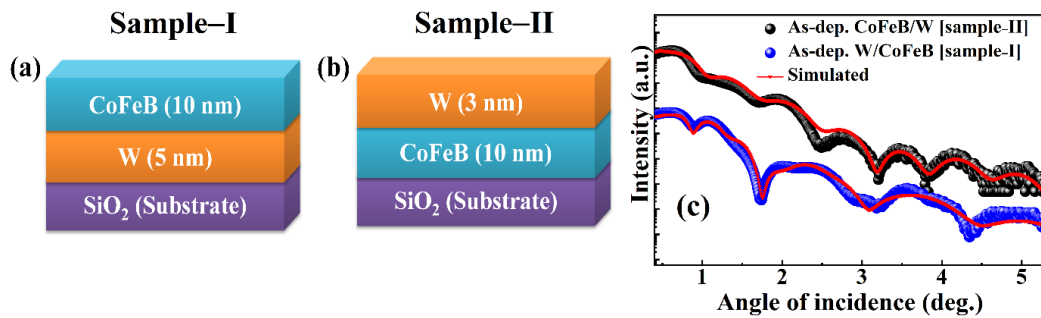


Fig.1 Schematic representation of the two types of heterostructures investigated in our experiment: (a) W/CoFeB and (b) CoFeB/W samples [labeled as sample-I and sample-II] and (c) The observed and simulated X-ray reflectivity spectrum of as-dep. heterostructures of samples-I and II.

The persistent presence of Kiessig fringes (XRR oscillations) up to $2\theta \approx 6^\circ$ indicates the films' high surface quality and relationship with the interface. The thickness, film density, and roughness interface of the as-dep. samples were determined by fitting experimentally obtained XRR profiles (see Table 1). The density of each layer is determined to be either very close to or slightly smaller than their respective bulk values. The measured thickness of individual layers matches the nominal thickness values. The overall interface roughness is less than 0.8 nm, indicating the excellent quality of these CoFeB films sputtered under high vacuum conditions. The analysis of the XRR profiles indicates a significant increase in interface width between CoFeB and W or Ta with crystallization [29].

Table 1. The fitted parameters for the thickness (t), density (Γ), and interface roughness (σ_i) of an as-dep. $\text{SiO}_2/\text{W}(5\text{nm})/\text{CoFeB}(10\text{nm})$ and $\text{SiO}_2/\text{CoFeB}(10\text{nm})/\text{W}(3\text{nm})$ films.

Sample	Simulated Parameters	Layers				
		SiO ₂	W	CoFeB	W	Oxide layer
W/CoFeB	Γ (g/cc)	2.12 ± 0.03	18.12 ± 0.08	6.7 ± 0.6	---	1.51 ± 0.03
	t(nm)	565 ± 14	5.2 ± 0.3	10.5 ± 0.6	---	1.33 ± 0.05
	σ_i (nm)	0.23 ± 0.03	0.41 ± 0.06	0.49 ± 0.06	---	0.41 ± 0.03
CoFeB/W	Γ (g/cc)	2.764	---	7.0 ± 0.5	16.78 ± 0.05	1.54 ± 0.02
	t(nm)	521 ± 12	---	9.3 ± 0.6	2.7 ± 0.2	0.93 ± 0.03
	σ_i (nm)	0.14 ± 0.01	---	0.32 ± 0.05	0.31 ± 0.04	0.72 ± 0.06

3.2 Structural analysis

The GI-XRD patterns were obtained from all the as-dep. CoFeB (10 nm) films indicate their amorphous nature and no distinct intensity signals corresponding to CoFeB or W films were observed (see Fig. 2). This amorphous characteristic is further supported by HR-TEM analysis conducted by M. Raju *et al.* [29]. Ref [27] shows that all the *ex-situ* annealed W(5 nm)/Co₂₀Fe₆₀B₂₀(10 nm)/W(3 nm) trilayer samples displayed a prominent crystalline peak corresponding to the (110) plane at $2\theta \approx 45^\circ$ which is indicative of the CoFe crystalline phase. Additionally, Nanhe *et al.* observed that *in-situ* annealed Ta (12 nm)/Co₆₀Fe₂₀B₂₀(28 nm)/Ta (5 nm) trilayer samples exhibited an amorphous nature up to temperatures of $\leq 400^\circ\text{C}$. However, annealing at temperatures $\geq 415^\circ\text{C}$ resulted in the transformation of CoFeB from an amorphous to a crystalline CoFe phase [29].

In our system, samples-I and II annealed at 400°C show polycrystalline bcc-CoFe, as evidenced by diffraction patterns at $2\theta = 44.9^\circ$, attributed to the (110) plane. The crystallite size of CoFe is determined by the Debye-Scherrer formula,

$$D = \frac{K\lambda}{\beta \cos \theta} \quad (1)$$

where D, K, λ , and β are the average crystallite size, a constant related to the size distribution, X-ray wavelength, and full width at half maximum of the peak, respectively [30]. The

average crystallite size of CoFe was determined to be ~ 18 nm and ~ 11 nm for samples-I and II at 400°C , respectively, and this result is consistent with previous reports [27].

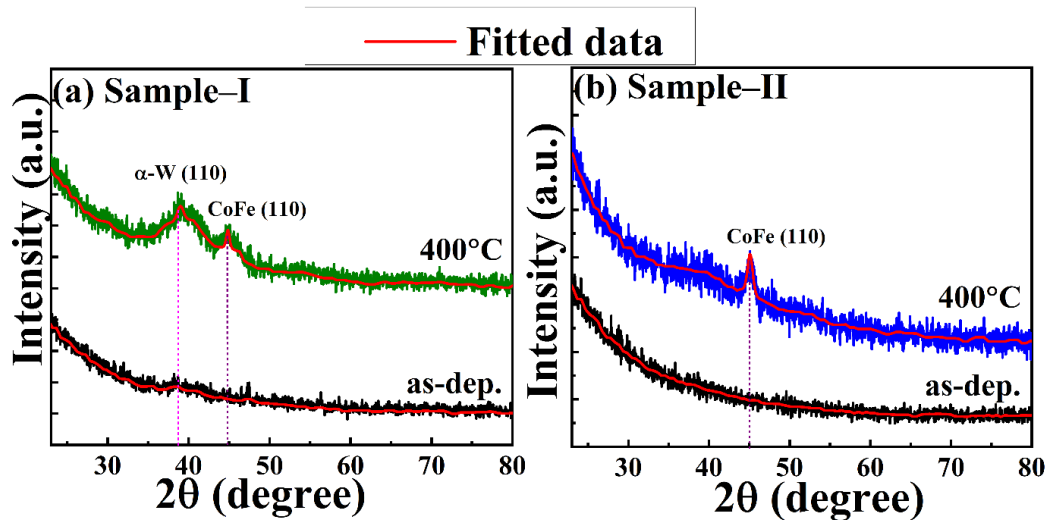


Fig.2 GI-XRD patterns for (a) sample-I and (b) sample-II and both sputtered at RT (as-dep.) and followed by annealing at 400°C .

The W buffer and capping layers influence the crystallite size variation in CoFeB films at 400°C . The crystalline phase is more pronounced in the W/CoFeB bilayer compared to the CoFeB/W bilayer. XRD analysis also reveals the presence of the α -W phase with a crystallite size of ~ 9 nm in the sample-I at 400°C and indicates a stable α -W phase formed on thermally oxidized Si substrates for thicker (5 nm) W films. This result aligns with previous reports [30,31] showing that sputtered W films' phase and resistivity depend on deposition conditions, temperature and thickness.

3.3 Magnetic anisotropy properties

3.3.1 In-plane magnetic anisotropy: L-MOKE

To study the magnetic anisotropy in W/CoFeB and CoFeB/W bilayers under various temperature conditions, we investigated the magnetization reversal of the samples using MOKE with an external magnetic field applied in both easy and hard axis directions. The in-plane angle-dependent MOKE hysteresis curves were recorded at RT from 0° to 360° with a step size 10° for both as-dep. and annealed (at 400°C) W(5 nm)/CoFeB(10 nm) and CoFeB(10 nm)/W(3 nm) samples. The results (see Fig. 3) suggest significant magnetic anisotropy exists in the sample-I at 400°C . The changes in in-plane coercivity depend on various factors such as defects pinning the motion of domain walls, the extent of oxidation,

crystallite size distribution, the creation of voids between grains, and so on [32,33]. The magnetization reversal in CoFe films was reported previously [34].

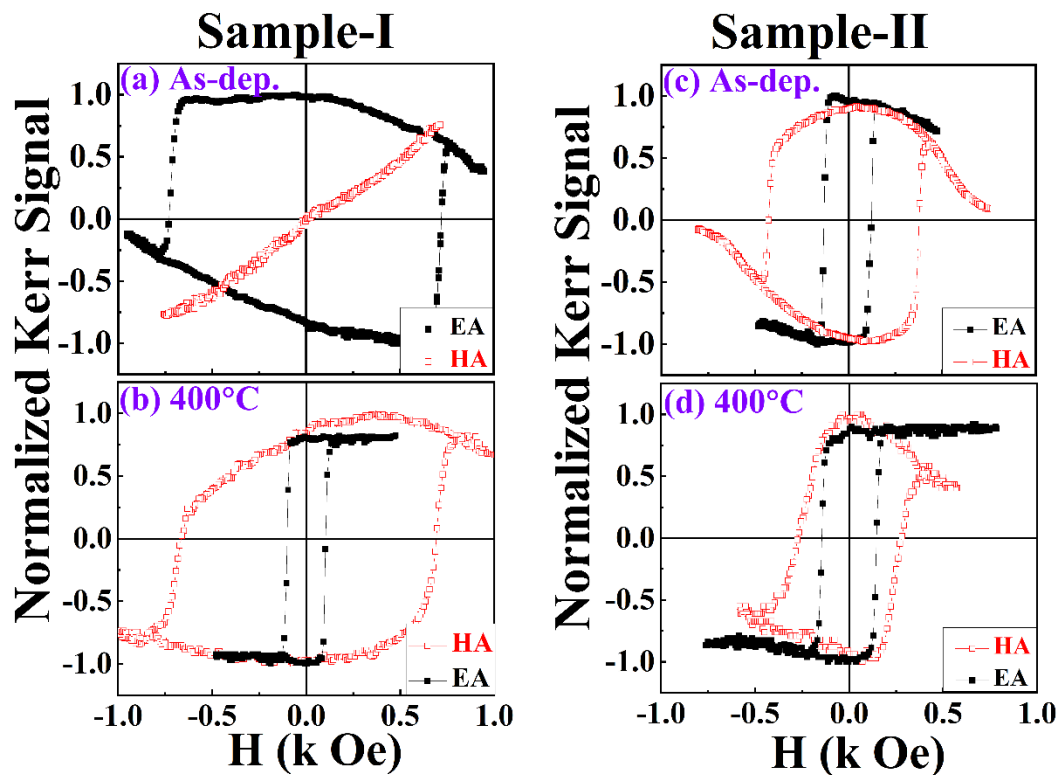


Fig.3 (a)-(d) MOKE M-H hysteresis loops recorded on samples–I and II in both the as-dep. and they annealed (400°C) states for two field orientations corresponding to the application of external magnetic field along the in-plane easy (black colour solid-squared data symbols) and hard axes (red colour open-squared data symbols). Lines are a guide to the eye.

The MOKE hysteresis loops corresponding to cases where the field is applied along the in-plane easy axis (*EA*) and hard axis (*HA*) of various W/CoFeB and CoFeB/W bilayers are shown in Fig. 3(a)-(d). For sample–I grown at RT, a large in-plane coercivity ($H_{c//}$) in the hysteresis loops was recorded along the easy axis [in-plane $H_{//} EA$], contrasting with the absence of $H_{c//}$ observed for the hard axis [in-plane $H_{//} HA$]. In the 400°C annealed sample–I, a small $H_{c//}$ of M-H loops was recorded along the easy axis, whereas a large $H_{c//}$ was obtained along the hard axis, as shown in Fig. 3(b). Moreover, a small $H_{c//}$ of hysteresis curves was again observed along the easy axis for sample–II at 400°C films (Fig. 3(d)). Previous reports [34] indicated that variations in the $H_{c//}$ value along the easy direction mainly depend on manipulating parameters such as pinning holes, sputtering bias voltage, crystallite size,

deposition rates of the films, etc. Additionally, local structural properties such as alterations in the grain sizes, defects, and strain [35] also affect the $H_{c//}$ and $M_r/M_{s//}$.

Figure 4(a)-(d) shows the angular-dependent $M_r/M_{s//}$ values of samples–I and II at RT and annealed at 400°C. This elucidates a consistent two-fold symmetry with differing shapes. From this analysis, we infer that the angular dependent $M_r/M_{s//}$ in the samples–I and II [both as-dep. and at 400°C] show well-defined strong magnetic anisotropy with two-fold symmetry. The detailed observation of two-fold anisotropy with various shapes was reported previously [27,36]. This in-plane UMA with two-fold symmetry is often observed in sputtered amorphous CoFe-based alloy systems and is believed to arise from strain effect and an anisotropic chemical disorder [37].

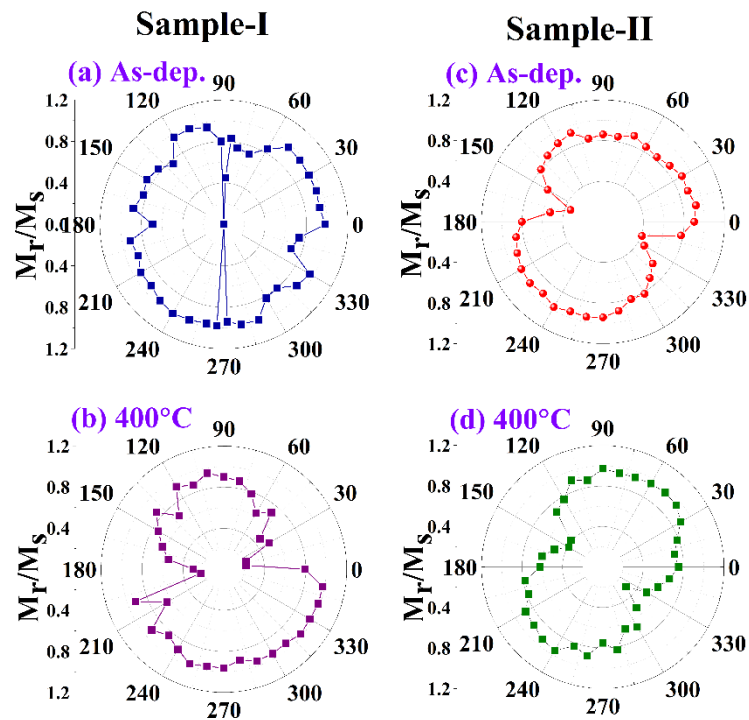


Fig.4 (a)-(d) Angular dependence of normalized M_r/M_s as a function of the applied field orientation for the sample–I and sample–II bilayer samples at RT and after annealing at 400°C. These samples demonstrate uniaxial symmetry along both the easy and hard axes.

3.3.2. In-plane and out-of-plane magnetic anisotropy: VSM

We further investigated the magnetic anisotropy (in-plane and out-of-plane directions) properties of the CoFeB film with W buffer and capping layers to assess the influence of T_A changes on the magnetostatic properties. The magnetic measurements were performed at RT

utilizing a VSM by applying magnetic field strengths ranging from +5.0 kOe to -5.0 kOe in parallel/in-plane and perpendicular/out-of-plane orientations of the film's surface. Figs. 5(a)-(d) presents the normalized M-H loops of both as-dep. and 400°C annealed samples–I and II. All the bilayer films exhibit low coercivity along the in-plane direction, corresponding to the easy axis of magnetization. In contrast, the hysteresis curves along the out-of-plane direction show high coercivity, indicating it serves as the hard axis of magnetization. The anisotropy field (H_k) was estimated from the hard axis saturation field measured at the intersection of in-plane and out-of-plane hysteresis loops [38,39]. The positive and negative signs of the H_k indicate the presence of PMA and in-plane magnetic anisotropy (IPA), respectively. The parallel and perpendicular M-H curves of samples–I and II at RT are displayed in Fig. 5 (a) and (c), respectively and all our bilayer samples exhibit IPA properties. The W buffer and capping layers significantly influence the strength of the H_k for the CoFeB film and are evidenced by the H_k values of -1.92 ± 0.08 kOe for as-dep. sample–I and -1.82 ± 0.07 kOe for as-dep. sample–II. A similar trend is observed at a T_A of 400°C for sample–I and sample–II as shown in Fig. 5 (b) and (d) [H_k values of -2.6 ± 0.1 kOe and -2.05 ± 0.08 kOe are observed for samples–I and II, respectively].

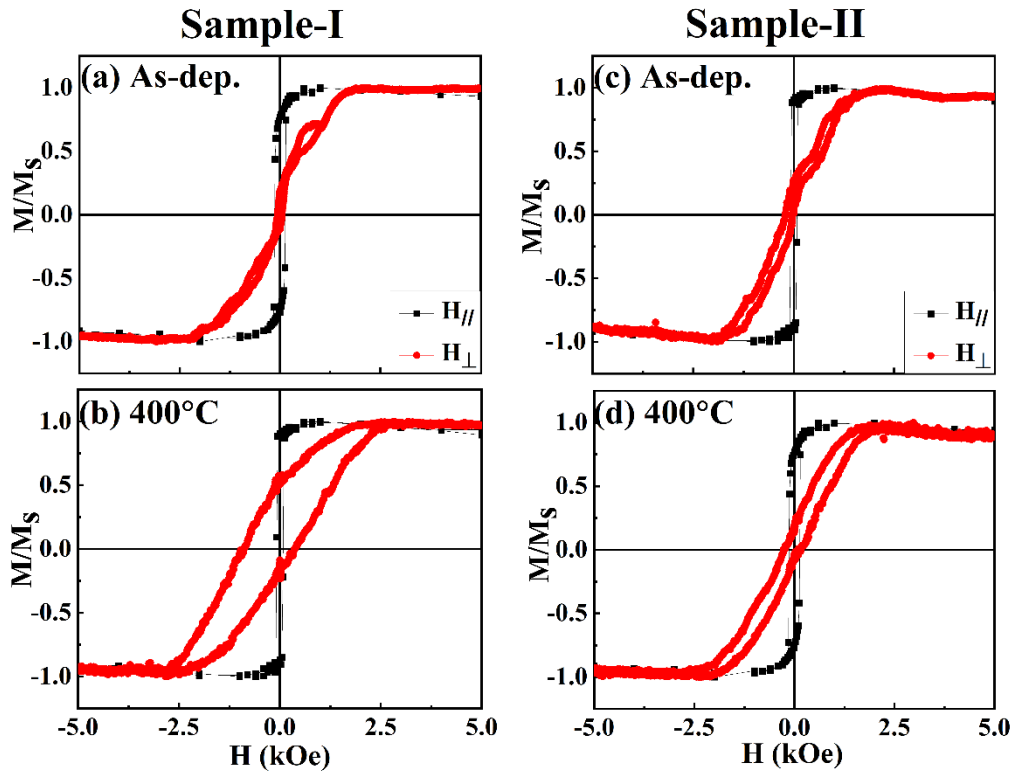


Fig.5 (a) & (c) Hysteresis loops of sample–I and sample–II in the as-dep. state, (b) & (d) sample–I and sample–II annealed at $T_A = 400^\circ\text{C}$.

Annealing at an appropriate temperature can rearrange the constituent elements at the interfaces, thereby minimizing the disorders that may have formed during deposition [40]. Therefore, the optimum T_A is crucial to adjusting the magnetic anisotropy in the films [37]. The H_{cL} of the sample-I was found to be 52 ± 2 Oe and 636 ± 25 Oe for as-dep. and 400°C annealed state, respectively. Similarly, for sample-II, H_{cL} values of 91 ± 3 Oe and 206 ± 9 Oe were determined for the as-dep. and 400°C annealed states, respectively. The H_{cL} values of a 400°C annealed sample are several times larger than those in the as-dep. state. A larger H_{cL} is observed for sample-I compared to sample-II at 400°C, which could be attributed to the W buffer layer promoting the crystallization of CoFeB during annealing [27,29]. Similar effects of buffer and capping layers in CoFeB/MgO multilayers at different temperatures have been recently reported [41]. Moreover, the release of boron atoms from CoFeB film and its microstructure can significantly impact the H_{cL} and magnetic moment during heat treatment [25–27,29,42–44]. Boron atoms typically have a smaller atomic radius compared to Co, Fe, and W. This size difference results in higher mobility and faster diffusion of boron atoms relative to these elements. During annealing, the increased mobility of boron atoms induces changes in the magnetization behavior of the CoFeB film.

The crystalline phase of CoFeB in the W/CoFeB sample is more pronounced than in the CoFeB/W bilayer samples annealed at 400°C. This difference in intensity arises from the fact that nanocrystallites in the W/CoFeB sample exert tensile stress on the surrounding amorphous phase and vice versa [47,48]. Additionally, several other factors may contribute to the observed large H_{cL} in the W/CoFeB bilayer: i) some bond orientation order resulting from interfacial interaction with the W layer [45,46], ii) structural defects and changes in compositional homogeneities due to crystallization can hinder domain wall motion and may also contribute to increased coercivity, iii) grain size and surface roughness of the films could affect H_{cL} and perpendicular anisotropy [25,47], iv) domain nucleation, growth and annihilation, where the average sizes develop intensely and may correlate strongly with strong H_{cL} [48]. Mainly, magnetization reversal in the out-of-plane direction of the samples is likely generated by effectively single nucleation due to strong inter-granular coupling and a phenomenon significantly induced by using the W layer [49,50]. Therefore, such out-of-plane magnetization reversal could be more strongly facilitated in the W/CoFeB bilayer than in the CoFeB/W bilayer. L-MOKE results on the angular dependence of M_r/M_s for all the bilayer

samples at RT and 400°C (Fig. 4) revealed a relatively stronger two-fold magnetic anisotropy in the annealed W/CoFeB bilayer than in the CoFeB/W system.

The release of boron from the CoFeB into the interface can lead to the formation of boron oxide and a well-ordered CoFe crystal structure under thermal treatment, which is one of the critical aspects primarily enhancing the H_{c1} [25]. In consequence, the H_{c1} in the CoFeB film is strongly influenced by the choice of buffer and capping layers [24,25,27].

The K_{eff} is obtained by [51],

$$K_{eff} = \frac{M_S H_K}{2} \quad (2)$$

To understand the strength of interfacial in-plane anisotropy in CoFeB films, we investigated the dependence of K_{eff} on T_A for W/CoFeB and CoFeB/W bilayers. The K_{eff} depends on both K_u and saturation magnetization (M_s), as indicated in equation (3), representing the cumulative impact of multiple anisotropy contributions on K_{eff} ,

$$K_{eff} = K_U - 2\pi M_S^2 \quad (3)$$

where,

$$K_U = \left[K_V + \left(\frac{2K_i}{t} \right) + \left(\frac{3}{2} \lambda \sigma \right) \right] \quad (4)$$

Here, t represents the thickness of the magnetic layer. Breaking down equations (3) and (4), the right-hand side comprises four distinct terms, each contributing to the overall K_{eff} of the system. In equation (4), the first term corresponds to volume magnetic anisotropy (K_v), which is linked to the crystallographic structure of the multilayer. The second term represents interface/surface magnetic anisotropy (K_i), arising from the interaction between electronic $d-p$ and $d-d$ states at the interfaces of different layers such as HM/FM/oxide or HM/FM [52]. The third term accounts for magnetoelastic anisotropy with ' σ ' and ' λ ' denoting the stress and magnetostriction constants. This term captures how mechanical stress and strain affect the material's magnetic properties [38,53]. Lastly, the fourth term in equation (3) denotes shape anisotropy $-2\pi M_S^2$ and favors an easy-plane anisotropy. This term accounts for the demagnetization energy associated with the film's shape and influences the preferred orientation of magnetization within the sample [54,55]. According to equation (3), a negative value of K_{eff} indicates a preference for the easy axis of magnetization to align parallel to the

plane within the samples, suggesting that demagnetization energy dominates over PMA. Conversely, a positive value of K_{eff} suggests that the easy axis of magnetization tends to align perpendicular to the plane.

As shown in Table 2, the IPA gets stronger when the films are annealed from RT to 400°C for both samples–I and II. With the increase in T_A , K_{eff} initially exhibits a higher value and then decreases. The maximum negative K_{eff} value is estimated at $-8.1 \pm 0.3 \times 10^5$ erg/cc for sample–I annealed at 400°C. A similar trend is observed for sample–II annealed at 400°C, with the maximum negative K_{eff} value of $-5.8 \pm 0.2 \times 10^5$ erg/cc. Similar changes in the magnetic and structural properties were recorded in CoFeB film-based stacks [29,37,51].

Table 2. In-plane and out-of-plane H_c , H_k , and K_{eff} for samples–I and II at various temperatures, especially as-dep. and 400°C.

S.No	Sample ID	T_A (°C)	Magnetic properties			
			$H_{c//}$ (Oe)	$H_{c\perp}$ (Oe)	H_k (k Oe)	K_{eff} ($\times 10^5$ erg/cc)
1	I	As-dep.	134±5	52±2	-1.92 ±0.08	-5.4 ±0.2
2		400	78±3	636±25	-2.6 ±0.1	-8.1 ±0.3
3	II	As-dep.	78±3	91±3	-1.82 ±0.08	-5.6 ±0.2
4		400	132±5	206±9	-2.06 ±0.08	-5.8 ±0.2

3.4 Topological analysis

The surface morphology of samples–I and II was investigated by operating AFM in tapping mode within a scan range of $5 \times 5 \mu\text{m}^2$ and a scale range of $1 \times 1 \mu\text{m}^2$. The AFM images shown in Fig. 6 demonstrate the impact of T_A on the bilayer films. The variations in surface morphology, surface roughness (R_{rms}), and grain size as a function of T_A are evident in both samples–I and II. For the as-dep. and 400°C annealed sample–I, distinct topographies are observed: the as-dep. sample displays individual, nearly spherical grains ranging from ≈ 118 nm to ≈ 142 nm (Fig. 6(a)), while the 400°C annealed sample shows rod-shaped grains as displayed in Fig. 6(b). In contrast, the as-dep. sample–II features spherical grains of ≈ 72 nm in size. The annealed sample–II exhibits larger agglomerated grains of ≈ 332 nm (Fig. 6(d)), which indicates that the post-annealing process led to agglomeration and further crystallization. The grain size and morphology can influence the coercivity of the films for

both applied field orientations (in-plane and out-of-plane) with rod-shaped or larger grains responsible for higher coercivity. This observation aligns with earlier reports [27,56,57].

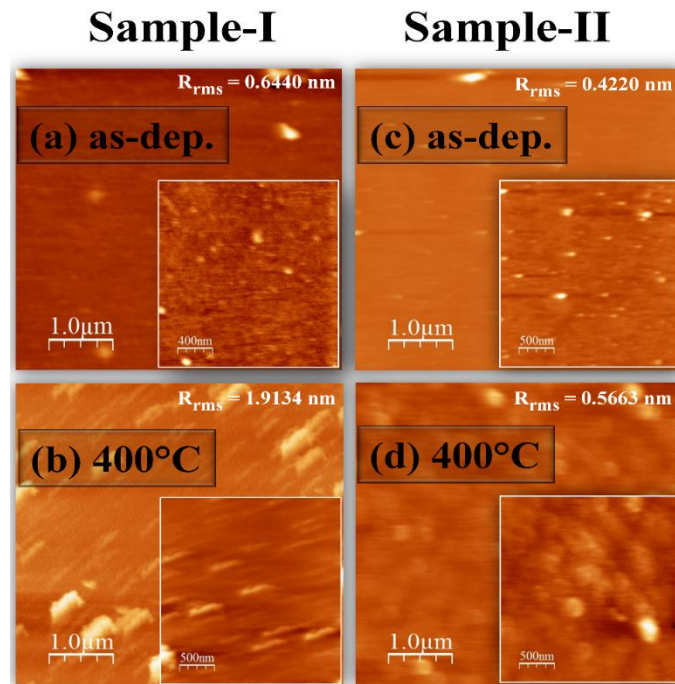


Fig.6 AFM images captured on the surface of the bilayer films in both as-dep. and 400°C annealed states: [(a)-(b)] for sample-I and [(c)-(d)] for sample-II.

The R_{rms} values for the as-dep. and 400 °C annealed W/CoFeB films are ≈ 0.64 nm and ≈ 1.91 nm, respectively. Similarly, R_{rms} values of ≈ 0.42 nm at RT/as-dep. and ≈ 0.57 nm at 400°C were observed for the CoFeB/W samples. The lowest interface/surface roughness is observed in the as-dep. sample-II, while an abrupt increase in roughness occurs at higher T_A . Generally, annealing promotes surface smoothness in materials. However, an increase in R_{rms} at higher annealing temperatures could also occur, as was observed in our case. This increase is often attributed to the coalescence of large-sized crystallites and/or the growth of grain size [58]. Additionally, the surface roughness and grain size can influence H_{cL} [25,47]. On the other hand, the absence of a capping layer in the sample-I may result in slight oxidation, which could alter the grain size on the surface.

The interface and surface roughness values obtained from XRR fitting (see Table 1) and AFM analysis show a similar trend across the samples-I and -II sequences. It is worth noting that interface roughness comparisons were made exclusively for the as-dep. samples-I and -II bilayers. Additionally, an oxide layer is present in both as-dep. samples-I and-II.

We claim the presence of magnetic anisotropy in our as-dep. amorphous W/CoFeB and CoFeB/W samples based on bond-orientational anisotropy (BOA). The structural anisotropy arising from the anisotropic structure factor and pair distribution function in binary or multi-component glassy systems was first reported by Suzuki *et al.* in $\text{Fe}_{40}\text{Ni}_{40}\text{Mo}_3\text{Si}_{12}\text{B}_5$ [59]. They linked this structural feature to atomic BOA, induced by stresses, where more atomic bonds align in one direction than perpendicular in glassy and amorphous solids. Harris *et al.* later confirmed BOA in sputtered amorphous Tb-Fe films and tied it to the uneven distribution of Fe-Fe, Tb-Tb, and Fe-Tb pairs within the film plane versus perpendicular orientations, which induces magnetic anisotropy in the film [60]. Such microscopic structural differences are inevitable in thin-film systems due to growth kinetics and associated strain and stress.

The magnetization anisotropy in amorphous CoFeB films grown via a magnetron sputtering system has been attributed to BOA and influenced by variations in composition (particularly boron) and thickness [45]. Considering the comparable energy kinetics observed during the growth of our samples, we consider that the exact BOA mechanism could also occur in our as-dep. W/CoFeB and CoFeB/W samples. In contrast, the annealed samples feature fewer but larger grains. This change leads to significant enhancements in nucleation and/or domain wall pinning and a substantial increase in anisotropy, possibly resulting in greater coercivity [27,48,61,62]. Consequently, the annealed CoFeB and W-based samples with larger grains exhibit higher coercivity than the as-dep. samples with smaller grains. Specifically, in our case, the grain size in the W/CoFeB annealed at 400°C is larger than that of CoFeB/W annealed at the same temperature. The annealing temperature of 400°C is energetically more favorable for segregating boron, resulting in a reduced boron content and altered magnetic moment in CoFeB. This observation is consistent with our XRD and VSM results.

4. SUMMARY AND CONCLUSION

In summary, the role of the tungsten buffer and capping layers in CoFeB film at a suitable temperature of 400°C emerges as a crucial factor in controlling the desired UMA properties. We have observed out-of-plane coercivity and UMA in as-dep. and annealed at 400°C optimal annealed W/CoFeB and CoFeB/W bilayers with a 10 nm thick CoFeB film. A large H_{cL} of 636 ± 25 Oe with two-fold symmetry UMA is observed for the W/CoFeB bilayer annealed at 400°C. The presence of large H_{cL} could have originated due to CoFeB crystallization, domain nucleation, and variations in microstructure during annealing. The annealing and the presence of buffer and capping layers of W considerably modify the UMA energy and create competition between H_{cL} and in-plane UMA. A maximum in-plane K_{eff} of $8.1 \pm 0.3 \times 10^5$ erg/cc is achieved for the W/CoFeB bilayer at 400°C sample. The α -W in the W/CoFeB bilayer annealed at 400°C enhances H_{cL} through various mechanisms, including crystal structure stability, enhancing magnetic anisotropy, exchange coupling, grain size and microstructural. This research explores a significant avenue for studying and developing the modern generation of ultra-low power storage applications, particularly in SOT-MRAM.

ACKNOWLEDGMENTS

L. Saravanan acknowledges the funding support from the FONDECYT Postdoctorado (2022), Agencia Nacional de Investigación y Desarrollo (ANID) (grant # 3220373). C. Garcia acknowledges the financial support ANID FONDECYT/Regular 1241918 and ANID FONDEQUIP EQM140161 received. This work was also supported by the European Union's Horizon 2020 research and innovation program under the Marie Skłodowska-Curie Grant Agreement No. 101007825 (ULTIMATE-I project).

REFERENCES

- [1] X. Fan, J. Wu, Y. Chen, M.J. Jerry, H. Zhang, J.Q. Xiao, Observation of the nonlocal spin-orbital effective field, *Nat Commun* 4 (2013) 1799. <https://doi.org/10.1038/ncomms2709>.
- [2] P. Jadaun, L.F. Register, S.K. Banerjee, The microscopic origin of DMI in magnetic bilayers and prediction of giant DMI in new bilayers, *Npj Comput Mater* 6 (2020) 88. <https://doi.org/10.1038/s41524-020-00351-1>.
- [3] G. Chen, A. Mascaraque, A.T. N'Diaye, A.K. Schmid, Room temperature skyrmion ground state stabilized through interlayer exchange coupling, *Applied Physics Letters* 106 (2015) 242404. <https://doi.org/10.1063/1.4922726>.
- [4] M.N. Wilson, A.B. Butenko, A.N. Bogdanov, T.L. Monchesky, Chiral skyrmions in cubic helimagnet films: The role of uniaxial anisotropy, *Phys. Rev. B* 89 (2014) 094411. <https://doi.org/10.1103/PhysRevB.89.094411>.
- [5] X. Qiu, K. Narayanapillai, Y. Wu, P. Deorani, D.-H. Yang, W.-S. Noh, J.-H. Park, K.-J. Lee, H.-W. Lee, H. Yang, Spin-orbit-torque engineering via oxygen manipulation, *Nature Nanotech* 10 (2015) 333–338. <https://doi.org/10.1038/nnano.2015.18>.
- [6] Q. Pan, Y. Liu, H. Wu, P. Zhang, H. Huang, C. Eckberg, X. Che, Y. Wu, B. Dai, Q. Shao, K.L. Wang, Efficient Spin-Orbit Torque Switching of Perpendicular Magnetization using Topological Insulators with High Thermal Tolerance, *Adv Elect Materials* 8 (2022) 2200003. <https://doi.org/10.1002/aelm.202200003>.
- [7] D. Pescia, Magnetism in ultrathin films, *Appl. Phys. A* 49 (1989) 437–437. <https://doi.org/10.1007/BF00617009>.
- [8] C.-J. Lin, G.L. Gorman, C.H. Lee, R.F.C. Farrow, E.E. Marinero, H.V. Do, H. Notarys, C.J. Chien, Magnetic and structural properties of Co/Pt multilayers, *Journal of Magnetism and Magnetic Materials* 93 (1991) 194–206. [https://doi.org/10.1016/0304-8853\(91\)90329-9](https://doi.org/10.1016/0304-8853(91)90329-9).
- [9] A. Maziewski, J. Fassbender, J. Kisielewski, M. Kisielewski, Z. Kurant, P. Mazalski, F. Stobiecki, A. Stupakiewicz, I. Sveklo, M. Tekielak, A. Wawro, V. Zablotskii, Magnetization states and magnetization processes in nanostructures: From a single layer to multilayers, *Physica Status Solidi (a)* 211 (2014) 1005–1018. <https://doi.org/10.1002/pssa.201300750>.
- [10] R. Skomski, *Simple Models of Magnetism*, Oxford University Press, 2008. <https://doi.org/10.1093/acprof:oso/9780198570752.001.0001>.
- [11] M.E. Buckley, F.O. Schumann, J.A.C. Bland, Strong changes in the magnetic properties of ultrathin Co/Cu(001) films due to submonolayer quantities of a nonmagnetic overlayer, *Phys. Rev. B* 52 (1995) 6596–6605. <https://doi.org/10.1103/PhysRevB.52.6596>.
- [12] L.A. Chebotkevich, Yu.D. Vorob'ev, A.S. Samardak, A.V. Ognev, Effect of the crystal structure and interlayer exchange coupling on the coercive force in Co/Cu/Co films, *Phys. Solid State* 45 (2003) 907–910. <https://doi.org/10.1134/1.1575333>.
- [13] T. Liu, J.W. Cai, L. Sun, Large enhanced perpendicular magnetic anisotropy in CoFeB/MgO system with the typical Ta buffer replaced by an Hf layer, *AIP Advances* 2 (2012) 032151. <https://doi.org/10.1063/1.4748337>.
- [14] D.-Y. Lee, T.-H. Shim, J.-G. Park, Effects of Pt capping layer on perpendicular magnet anisotropy in pseudo-spin valves of Ta/CoFeB/MgO/CoFeB/Pt magnetic-tunneling junctions, *Applied Physics Letters* 102 (2013) 212409. <https://doi.org/10.1063/1.4808084>.
- [15] I.-J. Shin, B.-C. Min, J.P. Hong, K.-H. Shin, Effects of Ru diffusion in exchange-biased MgO magnetic tunnel junctions prepared by *in situ* annealing, *Applied Physics Letters* 95 (2009) 222501. <https://doi.org/10.1063/1.3268791>.
- [16] T. Liu, Y. Zhang, J.W. Cai, H.Y. Pan, Thermally robust Mo/CoFeB/MgO trilayers with strong perpendicular magnetic anisotropy, *Sci Rep* 4 (2014) 5895. <https://doi.org/10.1038/srep05895>.
- [17] G.-G. An, J.-B. Lee, S.-M. Yang, J.-H. Kim, W.-S. Chung, J.-P. Hong, Highly stable perpendicular magnetic anisotropies of CoFeB/MgO frames employing W buffer and capping layers, *Acta Materialia* 87 (2015) 259–265. <https://doi.org/10.1016/j.actamat.2015.01.022>.

- [18] A. Natarajarathinam, Z.R. Tadisina, T. Mewes, S. Watts, E. Chen, S. Gupta, Influence of capping layers on CoFeB anisotropy and damping, *Journal of Applied Physics* 112 (2012) 053909. <https://doi.org/10.1063/1.4749412>.
- [19] M. Belmeguenai, M.S. Gabor, Y. Roussigne, F. Zighem, S.M. Cherif, C. Tiusan, Perpendicular Magnetic Anisotropy in Co₂FeAl Thin Films: Effect of Annealing Temperature, *IEEE Trans. Magn.* 51 (2015) 1–4. <https://doi.org/10.1109/TMAG.2015.2435815>.
- [20] Z. Wen, H. Sukegawa, S. Kasai, M. Hayashi, S. Mitani, K. Inomata, Magnetic Tunnel Junctions with Perpendicular Anisotropy Using a Co₂FeAl Full-Heusler Alloy, *Appl. Phys. Express* 5 (2012) 063003. <https://doi.org/10.1143/APEX.5.063003>.
- [21] H. Sukegawa, J.P. Hadorn, Z. Wen, T. Ohkubo, S. Mitani, K. Hono, Perpendicular magnetic anisotropy at lattice-matched Co₂FeAl/MgAl₂O₄(001) epitaxial interfaces, *Applied Physics Letters* 110 (2017) 112403. <https://doi.org/10.1063/1.4978663>.
- [22] K. Suemitsu, Y. Kawano, H. Utsumi, H. Honjo, R. Nebashi, S. Saito, N. Ohshima, T. Sugibayashi, H. Hada, T. Nohisa, T. Shimazu, M. Inoue, N. Kasai, Improvement of Thermal Stability of Magnetoresistive Random Access Memory Device with SiN Protective Film Deposited by High-Density Plasma Chemical Vapor Deposition, *Jjap* 47 (2008) 2714. <https://doi.org/10.1143/JJAP.47.2714>.
- [23] T. Kawahara, K. Ito, R. Takemura, H. Ohno, Spin-transfer torque RAM technology: Review and prospect, *Microelectronics Reliability* 52 (2012) 613–627. <https://doi.org/10.1016/j.microrel.2011.09.028>.
- [24] B. Sun, G.Q. Li, W.X. Zhao, Z. Shen, Y.H. Liu, P. Chen, Perpendicular coercive force of thick CoFeB thin films grown on silicon substrate, *Materials Letters* 123 (2014) 221–223. <https://doi.org/10.1016/j.matlet.2014.02.099>.
- [25] S. Lakshmanan, S.K. Rao, M.R. Muthuvel, G. Chandrasekaran, H.A. Therese, Variable substrate temperature deposition of CoFeB film on Ta for manipulating the perpendicular coercive forces, *Journal of Magnetism and Magnetic Materials* 435 (2017) 81–86. <https://doi.org/10.1016/j.jmmm.2017.03.069>.
- [26] L. Saravanan, M.M. Raja, D. Prabhu, H.A. Therese, Effect of thickness on tuning the perpendicular coercivity of Ta/CoFeB/Ta trilayer, *J Mater Sci: Mater Electron* 29 (2018) 336–342. <https://doi.org/10.1007/s10854-017-7921-3>.
- [27] L. Saravanan, N.K. Gupta, L. Pandey, I.P. Kokila, H.A. Therese, S. Chaudhary, Observation of uniaxial magnetic anisotropy and out-of-plane coercivity in W/Co₂₀Fe₆₀B₂₀/W structures with high thermal stability, *Journal of Alloys and Compounds* 895 (2022) 162600. <https://doi.org/10.1016/j.jallcom.2021.162600>.
- [28] B. Bhusan Singh, S. Chaudhary, Effect of MgO spacer and annealing on interface and magnetic properties of ion beam sputtered NiFe/Mg/MgO/CoFe layer structures, *Journal of Applied Physics* 112 (2012) 063906. <https://doi.org/10.1063/1.4752264>.
- [29] N. Kumar Gupta, S. Husain, V. Barwal, S. Hait, L. Pandey, V. Mishra, L. Saravanan, A. Kumar, N. Sharma, N. Kumar, S. Kumar Kedia, S. Chaudhary, Critical role of post-annealing in Ta/Co₆₀Fe₂₀B₂₀/Ta thin film heterostructures: Structural, static, and dynamic properties, *Journal of Magnetism and Magnetic Materials* 562 (2022) 169799. <https://doi.org/10.1016/j.jmmm.2022.169799>.
- [30] C.-F. Pai, L. Liu, Y. Li, H.W. Tseng, D.C. Ralph, R.A. Buhrman, Spin transfer torque devices utilizing the giant spin Hall effect of tungsten, *Appl. Phys. Lett.* 101 (2012) 122404. <https://doi.org/10.1063/1.4753947>.
- [31] J.-S. Lee, J. Cho, C.-Y. You, Growth and characterization of α and β -phase tungsten films on various substrates, *Journal of Vacuum Science & Technology A: Vacuum, Surfaces, and Films* 34 (2016) 021502. <https://doi.org/10.1116/1.4936261>.
- [32] W.W. Mullins, Theory of Thermal Grooving, *Journal of Applied Physics* 28 (1957) 333–339. <https://doi.org/10.1063/1.1722742>.
- [33] Y.-T. Chen, J.-Y. Tseng, T.-S. Sheu, Y.C. Lin, S.H. Lin, Effect of grain size on magnetic properties and microstructure of Ni₈₀Fe₂₀ thin films, *Thin Solid Films* 544 (2013) 602–605. <https://doi.org/10.1016/j.tsf.2012.12.058>.

- [34] Kaushalya, S. Husain, V. Barwal, N.K. Gupta, S. Hait, S. Chaudhary, Tunable magnetic anisotropy in obliquely sputtered Co₆₀Fe₄₀ thin films on Si(100), *Physica B: Condensed Matter* 570 (2019) 1–5. <https://doi.org/10.1016/j.physb.2019.05.013>.
- [35] R. Gupta, A. Khandelwal, R. Ansari, A. Gupta, K.G.M. Nair, Investigation of structural and magnetic properties of nanoscale Fe/Co bilayers, *Surface and Coatings Technology* 203 (2009) 2717–2720. <https://doi.org/10.1016/j.surfcoat.2009.02.100>.
- [36] U. Urdirroz, B.M.S. Teixeira, F.J. Palomares, J.M. Gonzalez, N.A. Sobolev, F. Cebollada, A. Mayoral, Dynamic magnetic properties of amorphous Fe₈₀B₂₀ thin films and their relation to interfaces, *AIP Advances* 10 (2020) 015013. <https://doi.org/10.1063/1.5129996>.
- [37] K. Wang, Y. Huang, R. Chen, Z. Xu, Investigation of magnetic properties in thick CoFeB alloy films for controllable anisotropy, *Appl. Phys. A* 122 (2016) 98. <https://doi.org/10.1007/s00339-016-9633-6>.
- [38] M.T. Johnson, P.J.H. Bloemen, F.J.A.D. Broeder, J.J.D. Vries, Magnetic anisotropy in metallic multilayers, *Rep. Prog. Phys.* 59 (1996) 1409–1458. <https://doi.org/10.1088/0034-4885/59/11/002>.
- [39] A. Kaidatzis, C. Bran, V. Psycharis, M. Vázquez, J.M. García-Martín, D. Niarchos, Tailoring the magnetic anisotropy of CoFeB/MgO stacks onto W with a Ta buffer layer, *Applied Physics Letters* 106 (2015) 262401. <https://doi.org/10.1063/1.4923272>.
- [40] M. Li, J. Lu, G. Yu, X. Li, G. Han, X. Chen, H. Shi, G. Yu, P.K. Amiri, K.L. Wang, Influence of inserted Mo layer on the thermal stability of perpendicularly magnetized Ta/Mo/Co₂₀Fe₆₀B₂₀/MgO/Ta films, *AIP Advances* 6 (2016) 045107. <https://doi.org/10.1063/1.4947075>.
- [41] W. Du, M. Liu, F. Han, H. Su, B. Liu, H. Meng, X. Tang, Effect of Buffer and Cap Layer on Thermally Stable Perpendicular Magnetic Anisotropy in Buffer/CoFeB/MgO/Cap Structure, *IEEE Magn. Lett.* 13 (2022) 1–4. <https://doi.org/10.1109/LMAG.2022.3221050>.
- [42] M. Raju, S. Chaudhary, D.K. Pandya, Multi-jump magnetic switching in ion-beam sputtered amorphous Co₂₀Fe₆₀B₂₀ thin films, *Journal of Applied Physics* 114 (2013) 053911. <https://doi.org/10.1063/1.4817653>.
- [43] W.X. Wang, Y. Yang, H. Naganuma, Y. Ando, R.C. Yu, X.F. Han, The perpendicular anisotropy of Co₄₀Fe₄₀B₂₀ sandwiched between Ta and MgO layers and its application in CoFeB/MgO/CoFeB tunnel junction, *Applied Physics Letters* 99 (2011) 012502. <https://doi.org/10.1063/1.3605564>.
- [44] M. Yamanouchi, R. Koizumi, S. Ikeda, H. Sato, K. Mizunuma, K. Miura, H.D. Gan, F. Matsukura, H. Ohno, Dependence of magnetic anisotropy on MgO thickness and buffer layer in Co₂₀Fe₆₀B₂₀-MgO structure, *Journal of Applied Physics* 109 (2011) 07C712. <https://doi.org/10.1063/1.3554204>.
- [45] A.T. Hindmarch, A.W. Rushforth, R.P. Campion, C.H. Marrows, B.L. Gallagher, Origin of in-plane uniaxial magnetic anisotropy in CoFeB amorphous ferromagnetic thin films, *Phys. Rev. B* 83 (2011) 212404. <https://doi.org/10.1103/PhysRevB.83.212404>.
- [46] Q. Hao, W. Chen, G. Xiao, Beta (β) tungsten thin films: Structure, electron transport, and giant spin Hall effect, *Applied Physics Letters* 106 (2015) 182403. <https://doi.org/10.1063/1.4919867>.
- [47] F.-T. Yuan, Y.-H. Lin, J.K. Mei, J.-H. Hsu, P.C. Kuo, Effect of thickness of MgO, Co-Fe-B, and Ta layers on perpendicular magnetic anisotropy of [Ta/Co₆₀Fe₂₀B₂₀/MgO]₅ multilayered films, *Journal of Applied Physics* 111 (2012) 07C111. <https://doi.org/10.1063/1.3673408>.
- [48] A.G. Kolesnikov, M.E. Steblyy, A.V. Ognev, A.S. Samardak, A.N. Fedorets, V.S. Plotnikov, X. Han, L.A. Chebotkevich, Enhancement of perpendicular magnetic anisotropy and coercivity in ultrathin Ru/Co/Ru films through the buffer layer engineering, *J. Phys. D: Appl. Phys.* 49 (2016) 425302. <https://doi.org/10.1088/0022-3727/49/42/425302>.
- [49] W. Frost, M. Samiepour, A. Hirohata, Perpendicular Anisotropy Controlled by Seed and Capping Layers of Heusler-Alloy Films, *IEEE Trans. Electron Devices* 69 (2022) 1629–1633. <https://doi.org/10.1109/TED.2021.3105490>.
- [50] W. Frost, A. Hirohata, Heusler alloys with bcc tungsten seed layers for GMR junctions, *Journal of Magnetism and Magnetic Materials* 453 (2018) 182–185. <https://doi.org/10.1016/j.jmmm.2018.01.015>.

- [51] L. Kipgen, H. Fulara, M. Raju, S. Chaudhary, In-plane magnetic anisotropy and coercive field dependence upon thickness of CoFeB, *Journal of Magnetism and Magnetic Materials* 324 (2012) 3118–3121. <https://doi.org/10.1016/j.jmmm.2012.05.012>.
- [52] B. Dieny, M. Chshiev, Perpendicular magnetic anisotropy at transition metal/oxide interfaces and applications, *Rev. Mod. Phys.* 89 (2017) 025008. <https://doi.org/10.1103/RevModPhys.89.025008>.
- [53] M.T. Johnson, R. Jungblut, P.J. Kelly, F.J.A. Den Broeder, Perpendicular magnetic anisotropy of multilayers: recent insights, *Journal of Magnetism and Magnetic Materials* 148 (1995) 118–124. [https://doi.org/10.1016/0304-8853\(95\)00174-3](https://doi.org/10.1016/0304-8853(95)00174-3).
- [54] J. Sort, V. Baltz, F. Garcia, B. Rodmacq, B. Dieny, Tailoring perpendicular exchange bias in [Pt/Co]-IrMn multilayers, *Phys. Rev. B* 71 (2005) 054411. <https://doi.org/10.1103/PhysRevB.71.054411>.
- [55] S. Bandiera, R.R. Sousa, B.B. Rodmacq, B. Dieny, Asymmetric Interfacial Perpendicular Magnetic Anisotropy in Pt/Co/Pt Trilayers, *IEEE Magn. Lett.* 2 (2011) 3000504–3000504. <https://doi.org/10.1109/LMAG.2011.2174032>.
- [56] W.S. Sun, T. Kulik, X.B. Liang, J. Ferenc, Thermal stability and magnetic properties of Co–Fe–Hf–Ti–Mo–B bulk metallic glass, *Intermetallics* 14 (2006) 1066–1068. <https://doi.org/10.1016/j.intermet.2006.01.026>.
- [57] Y.-T. Chen, C.C. Chang, Effect of grain size on magnetic and nanomechanical properties of Co₆₀Fe₂₀B₂₀ thin films, *Journal of Alloys and Compounds* 498 (2010) 113–117. <https://doi.org/10.1016/j.jallcom.2010.03.141>.
- [58] S.-S. Park, J.S. Bae, S. Park, The growth-temperature-dependent interface structure of yttria-stabilized zirconia thin films grown on Si substrates, *J. Phys.: Condens. Matter* 22 (2010) 015002. <https://doi.org/10.1088/0953-8984/22/1/015002>.
- [59] Y. Suzuki, J. Haimovich, T. Egami, Bond-orientational anisotropy in metallic glasses observed by x-ray diffraction, *Phys. Rev. B* 35 (1987) 2162–2168. <https://doi.org/10.1103/PhysRevB.35.2162>.
- [60] V.G. Harris, K.D. Aylesworth, B.N. Das, W.T. Elam, N.C. Koon, Structural origins of magnetic anisotropy in sputtered amorphous Tb-Fe films, *Phys. Rev. Lett.* 69 (1992) 1939–1942. <https://doi.org/10.1103/PhysRevLett.69.1939>.
- [61] Y. Sun, R. Gao, Effect of defects on the effective anisotropy and coercivity in nanometer hard magnetic materials, *Solid State Communications* 149 (2009) 393–395. <https://doi.org/10.1016/j.ssc.2008.12.015>.
- [62] J. Zhang, Y. Li, F. Wang, B. Shen, J. Sun, Coercivity mechanism of nanocomposite Sm-Co/Fe multilayer films, *Journal of Applied Physics* 107 (2010) 043911. <https://doi.org/10.1063/1.3309772>.

HIGHLIGHTS

- ❖ All W/CoFeB and CoFeB/W bilayer samples exhibited magnetic anisotropy with two-fold symmetry
- ❖ A large $H_{c\perp}$ of 636 ± 25 Oe and K_{eff} of $8.1 \pm 0.3 \times 10^5$ erg/cc for in-plane UMA is observed for W/CoFeB bilayer annealed at 400°C
- ❖ High $H_{c\perp}$ could result from improved CoFeB crystallization with α -W phase formation and annealing-induced microstructure alterations
